

Room-Temperature, Homogeneous, Single-Step, and Large-Scale Synthesis of Perovskite Nanoplatelets for Blue Light-Emitting Diodes

Ju-Hyun Yoo, Sungjin Kim, Hyeokjung Lee, Cheolmin Park, Tae-Woo Lee, and Jin-Woo Park*



Cite This: *ACS Appl. Mater. Interfaces* 2023, 15, 39461–39471



Read Online

ACCESS |

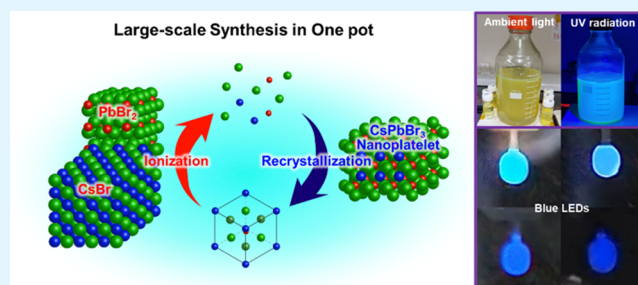
Metrics & More

Article Recommendations

Supporting Information

ABSTRACT: Inorganic perovskite nanocrystals (IPNCs) have attracted considerable attention due to their excellent optoelectronic properties. However, problems arise from anion migration during the preparation of a blue light-emitting diode (LED), and only small-scale syntheses have been conducted on a laboratory scale. By using only Br as the anion here, CsPbBr₃ was synthesized in the form of nanoplatelets to eliminate the effects of anion migration and to prepare an inorganic perovskite nanoplatelet (IPNPL) emitting blue light. In addition, the synthesis was performed under ambient conditions at room temperature, and the synthetic process was shortened to enable large-scale synthesis. We used a 1 L bottle for large-scale synthesis, and a photoluminescence quantum yield (PLQY) of 78% was observed at 460 nm. We fabricated LEDs by using IPNPLs, and we observed an electroluminescence peak at 461 nm. The developed synthetic method is expected to pave the way for commercialization of IPNCs and the next-generation display market.

KEYWORDS: perovskite nanoplatelets, blue light-emitting diodes, large-scale synthesis, one-pot method, room-temperature synthesis



INTRODUCTION

Lead halide perovskites (LHPs) have excellent optical properties, such as high photoluminescence quantum yields (PLQYs), light emission with narrow full width at half-maximum (fwhm) values, photostability, high light absorption, high defect tolerance, and tunable band gaps enabled by halogen ion substitution.^{1–8} Hence, LHPs have been extensively applied in various optoelectronic devices, including biological imagers, light-emitting diodes (LEDs), solar cells, photodetectors, and lasers.^{9–11} The PLQYs and external quantum efficiencies (EQEs) of LHPs are significantly enhanced when the LHPs form perovskite nanocrystals (PNCs).¹² When the sizes of the PNCs are less than the Bohr radius, quantum confinement takes effect and results in an increase in the exciton binding energy.¹³ Therefore, PNCs are suitable for use as light-emitting materials for LEDs.¹³

Red and green PNC-based LEDs (PeLEDs) synthesized in solution have recently been reported to have EQEs of 24.4 and 23.4%, respectively.^{8,14} In contrast, challenges remain for increasing the significantly lower EQEs of blue light-emitting PeLEDs, which are approximately 12.3%.¹⁵ One issue is that blue light-emitting organic–inorganic hybrid PNCs (HPNCs), which are easy to synthesize, have low thermal stabilities and are vulnerable to humidity.³ On the other hand, blue light-emitting inorganic PNCs (IPNCs) show better light emission performance than HPNCs due to their overall high stabilities to high temperatures and humidity.¹⁶ However, the low

solubilities of blue light-emitting IPNCs make it challenging to synthesize them on a large scale.¹⁶ Furthermore, the formation of defect states with large band gaps for blue light-emitting PNCs reduces their intrinsic photoluminescence (PL) efficiencies and electroluminescence (EL) efficiencies as blue light-emitting LEDs.¹⁶

One approach used to synthesize blue-emitting IPNCs involves mixing chlorine and bromine as the X components in the ABX₃ perovskite structure. However, the blue emission peaks of IPNCs are often red-shifted or merge into single components of multiplex emission spectra due to phase separation induced by halide ion migration.^{17–19} Hence, other researchers have explored reductions in at least one of the three dimensions for bromine-only IPNCs and the formation of nanostructures such as nanoplatelets (NPLs) to achieve induced quantum confinement.^{17–21} In CsPbBr₃, the exciton Bohr diameter is 7 nm, and quantum confinement occurs when the particle size is near or smaller than the exciton Bohr diameter. So, CsPbBr₃ NPLs consisting of a few monolayers

Received: March 6, 2023

Accepted: July 27, 2023

Published: August 9, 2023



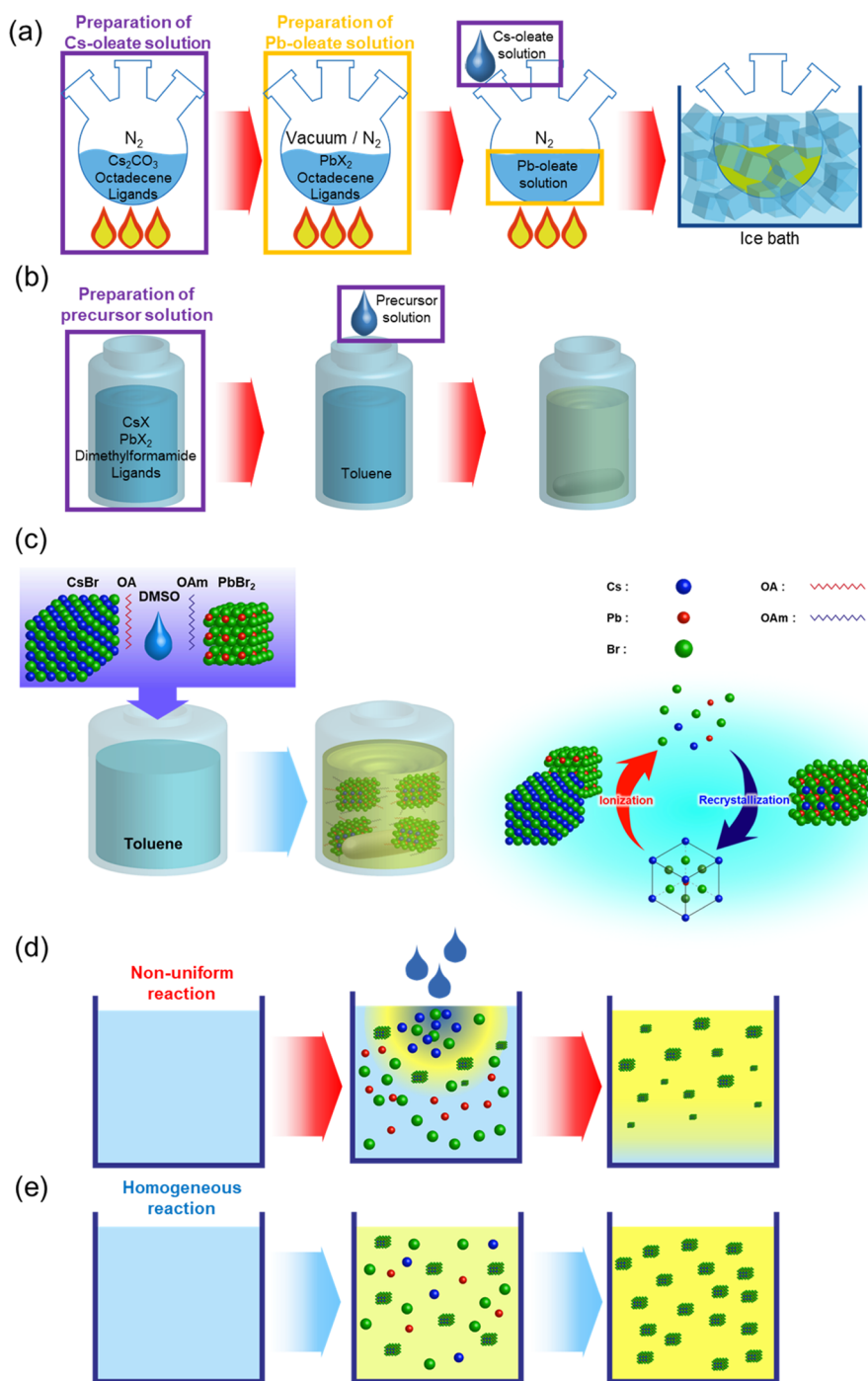


Figure 1. Schematic representations for (a) each step of the hot-injection method, (b) the ligand-assisted reprecipitation method, and (c) our new synthesis method that is room-temperature homogeneous IPNPL synthesis. Comparative schematics of (d) heterogeneous reactions using conventional methods in large-scale synthesis and (e) a homogeneous reaction using our new large-scale synthetic method.

(ML) exhibit blue emission.^{19,22,23} Inorganic perovskite NPLs (IPNPLs) containing a single type of halide ion are not affected by halide ion migration, and their emission peaks are affected only by NPL thickness.²⁴

The hot-injection (HI) and ligand-assisted reprecipitation (LARP) methods are the two most frequently used synthetic methods for preparing IPNCs, including IPNPLs.^{1,22,25} The most frequently used HI process produces IPNCs by injecting a cesium oleate precursor solution into a PbX₂ (X = I, Br, Cl) precursor solution at 140 to 200 °C (Figure 1a). CsPbX₃ (X = I, Br, Cl) IPNCs synthesized through HI that emit light

between 410 and 700 nm in the visible region showed narrow fwhm's of 12 to 42 nm and high PLQYs between 50 and 90%.²² Moreover, the emission peaks and sizes of the CsPbX₃ IPNCs can be easily controlled through anion exchange reactions and the choice of synthetic temperature, respectively.^{26,27} However, HI requires a high temperature and an inert gas atmosphere, thereby significantly increasing the cost of production.¹ Furthermore, it is difficult to control the various temperature requirements of the individual precursors and reduce the large temperature gradients generated in the

mixing process, which leads to increased complexity in large-scale processes using the HI method.^{1,28}

In contrast to HI, LARP reduces the cost of IPNC production because processing is performed at room temperature under ambient air (Figure 1b).^{1,25} In LARP, both CsX (X = I, Br, Cl) and PbX₂ are dissolved in N,N-dimethylformamide (DMF) to prepare a precursor solution, which is injected into a low-solubility solvent to synthesize IPNCs.^{1,25} Hence, LARP requires only a short time to synthesize IPNCs with high PLQYs exceeding 70% and narrow fwhm's of less than 35 nm.¹ However, because the two participating solvents lead to different solubilities, nonuniform mixing occurs in the LARP processes. The residual DMF used as a solvent for LARP can also damage or dissolve IPNCs, resulting in poor light emission performance.^{11,25,28,29}

Pan et al. performed the gram-scale synthesis of IPNCs at room temperature in open air by mixing Cs/Pb and Br precursor solutions to synthesize CsPbBr₃ IPNCs with a PLQY of 80%.²⁸ The synthesis was performed at room temperature, but a high temperature of 160 °C was required to prepare the precursor solutions.²⁸ Furthermore, initial contact of the two precursor solutions led to nonuniform formation of IPNCs since the combined solvent led to instant formation of IPNCs without allowing the participating ions to be distributed homogeneously. On the other hand, Wang et al. simultaneously added Cs₂CO₃ and PbBr₂ to a solution and heated them to synthesize CsPbBr₃ in one pot and on a gram scale.³⁰ This gram-scale synthesis resulted in CsPbBr₃ IPNCs with a PLQY of 77% and a fwhm of 21 nm.³⁰ However, although Wang et al. overcame the nonuniform mixing problem, they still employed a high-temperature process.³⁰

This study demonstrated that CsPbBr₃ IPNPLs could be synthesized in a single-step, one-pot approach at room temperature in ambient air (Figure 1c). The synthesis was performed in a homogeneous solution without additional preparation steps (Figure 1e). A slow, reversible ion reaction was induced to reduce the structural defects of CsPbBr₃ IPNPLs to exhibit uniform light emission. By adding two ligands (oleic acid and oleylamine) and a small amount of the good solvent dimethyl sulfoxide (DMSO) to the poor solvent toluene, ionization and recrystallization of the perovskite crystalline structure occurred repeatedly over several cycles during the synthetic process. Furthermore, the ligand concentrations were optimized such that the ligands facilitated the formation of the desired shape and thickness of the IPNCs for NPLs.

The single-step, one-pot approach used in this work under ambient conditions allowed for the homogeneous and steady-state formation of IPNPLs, unlike the significantly faster but nonuniform and uncontrollable syntheses reported previously. Hence, the approach demonstrated here was not affected by the size of the synthetic vessel, which enabled the large-scale and uniform synthesis of IPNPLs. The crystal structures and compositions of the IPNPLs were verified by using high-resolution X-ray diffraction (XRD) and transmission electron microscopy (TEM). Consequently, PL and EL spectra were used to characterize the light emission performance of the IPNPLs.

RESULTS AND DISCUSSION

New Synthetic Method. For the HI method (Figure 1a) and the LARP method (Figure 1b), precursors were prepared separately, as shown in Figure 1a,1b, and these precursor

solutions were then mixed together. After mixing, the solubility decreased rapidly and recrystallization occurred quickly, resulting in a short synthesis time. However, if the amount of precursors to be mixed was large, nanoparticles with nonuniform shapes and sizes were produced during crystallization (Figure 1d). Since the synthesis proceeded very quickly, if the amount of product to be synthesized was increased, a concentration gradient occurred when the precursor solutions were mixed. Accordingly, differences occurred in the sizes and shapes of the synthesized nanoparticles. It was challenging to control the concentrations during the synthesis, and as the scale of the synthesis was increased, complete mixing took longer.

To overcome this limitation for a large-scale synthesis, we eliminated the mixing step by performing the synthesis in one pot. We added a small amount of a polar solvent to provide high solubility to a mixed solution for the chemical reaction. We devised a synthetic method with which to convert the precursors into a perovskite structure through repeated ionization and recrystallization over time. All materials used for the synthesis were put into one pot, and DMSO was mixed with toluene to control the solubility. Ionization and recrystallization of CsBr and PbBr₂ occurred repeatedly over time due to the added ligands and DMSO. When the dissolved ions underwent recrystallization, they formed nanocrystals due to the presence of ligands (Figure 1c).

In previous synthetic methods, such as HI and LARP, the synthesis occurred when the two precursor solutions were mixed. However, the compositions of the mixed solution were different at each point due to the concentration gradient, which caused the formation of nonuniform nanocrystals. The solvent used for the precursor solution reionized the developed nanocrystals. In this study, nanocrystals were uniformly synthesized in solution by mixing all of the solvents in one pot.

In this one-pot synthetic method, we selected four factors based on a literature review and our preliminary experiments.^{11,31,32} We varied the following factors affecting the synthesis: (1) the ratio of Cs to Pb, (2) the amount of ligand added, (3) the amount of DMSO added, and (4) the synthesis time. Parametric studies were conducted using 5–10 sets of specimens for each factor (Tables S1–S5 in the Supporting Information), and we identified the primary and secondary parameters among the four factors. Although the synthesis temperature and the lengths of the ligands also affected the synthesis, the temperature was fixed at room temperature when synthesizing NPLs because our goal was room-temperature synthesis.³³ When we varied the lengths of the ligands in our previous preliminary experiments, the experimental conditions had to be changed for each length. Therefore, it was difficult to analyze the effects of ligand length on synthesis with the other conditions fixed. Hence, synthesis with ligands of varying lengths was excluded from the experiments.

A total of 0.32 mmol of CsBr, 0.4 mmol of PbBr₂, 0.1 mL of DMSO, 2 mL of OA, 0.9 mL of OAm, and 10 mL of toluene were used as the reference conditions for synthesizing NPLs. The synthesis time was 72 h based on our experimental results, and the PL efficiencies were measured after adjusting each variable. As shown in Tables S1–S5, we adjusted each variable to synthesize the NPLs. When CsPbBr₃ was prepared in the form of NPLs, the Cs-to-Pb ratio decreased to less than 1.³² The ligands ionized the compound in solution and allowed it to exist stably in its nanocrystalline form after recombination. In addition, by controlling the amounts of ligands, nanocrystals

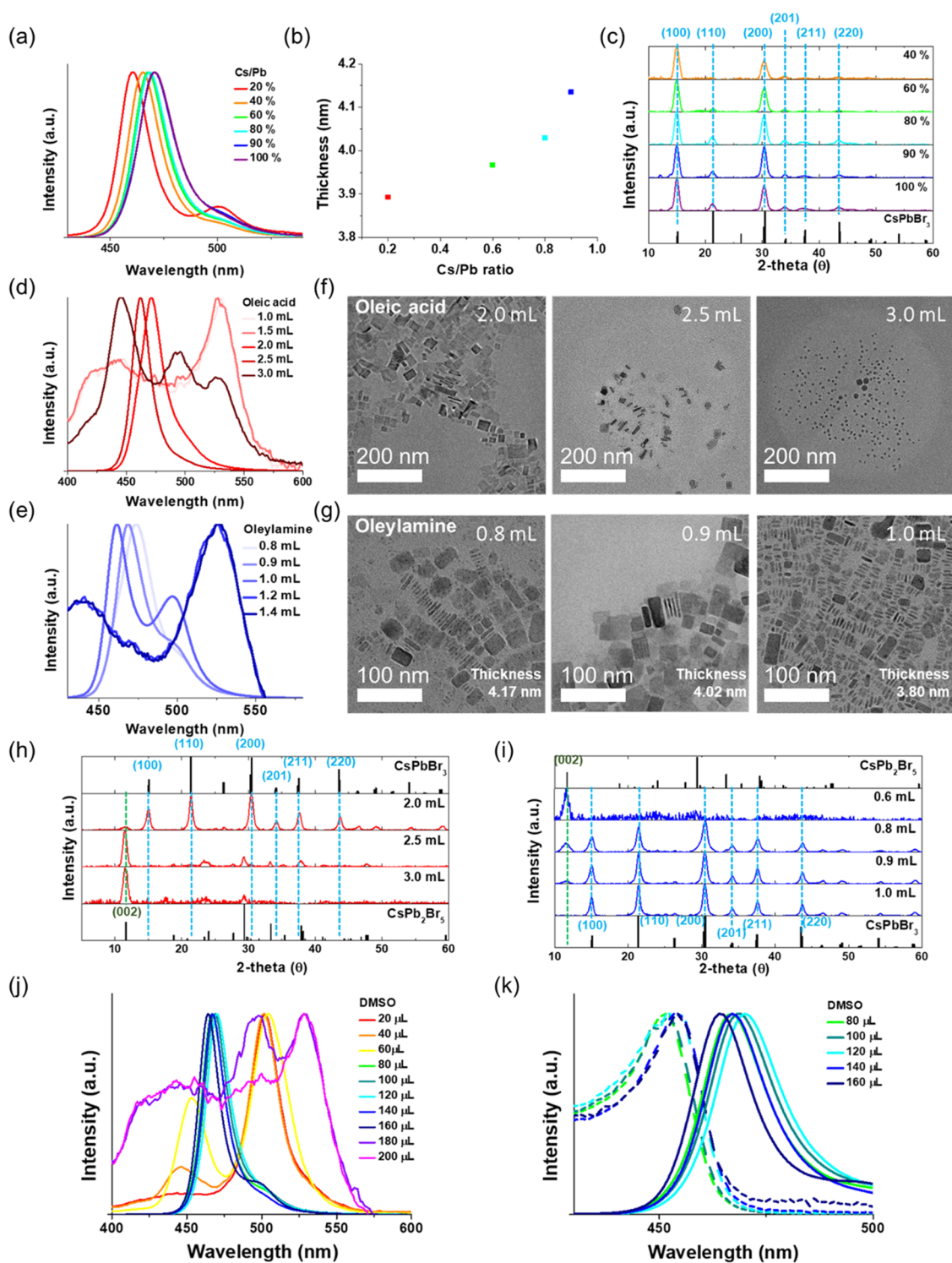


Figure 2. (a) PL spectra, (b) average thickness, and (c) XRD patterns of NPLs with different ratios of Cs/Pb. (d) PL spectra, (f) TEM images, and (h) XRD patterns of NPLs prepared with different amounts of oleic acid. (e) PL spectra, (g) TEM images, and (i) XRD patterns of NPLs prepared with different amounts of oleylamine. (j) PL spectra of NPLs synthesized by 3 days with different amounts of DMSO. (k) UV-vis absorption spectra and PL spectra of NPLs prepared with different amounts of DMSO.

were converted into NPLs.¹¹ Accordingly, the amount of cesium and the amounts of ligands used were adjusted to form NPLs.¹¹ As the amount of DMSO added increased, the synthesis rate increased. However, if the amount of DMSO used was too high, it was difficult to form nanoparticles. The low solubility of the solution resulted in a long synthesis time. The product was gradually synthesized in the form of NPLs

based on the synthesis time, and when the reaction was continued for too long after the synthesis was completed, larger particles were formed by the residual DMSO and ligands.

Controlling Factors for the Synthesis. *Ratio of Cs to Pb.* ABX₃ is the general formula for perovskites, but in the case of nanoparticles, various structural formulas exist depending on

the shapes.³² The structural formulas of the NPLs change according to the thickness, and the formula is expressed as $L_2[ABX_3]_{n-1}BX_4$.³² In the case of the cesium lead halide perovskite, cesium occupies site A, lead occupies site B, and the Cs-to-Pb ratio is 1:1.³² Nevertheless, in the case of the NPL shape, the proportion of the A site decreased as the thickness decreased.³² Therefore, we expected the thickness to change depending on the Cs-to-Pb ratio used in the synthesis.³³ We carried out syntheses by varying the ratios of Cs/Pb to confirm the effect on NPL thickness. According to our experimental results, the PL peak blue-shifted (Figure 2a) as the amount of cesium was decreased. This meant that the synthesized nanocrystals decreased in size or the NPLs became thinner.²⁰ We used TEM to determine whether the thickness of the NPLs changed by varying the Cs-to-Pb ratio (Figure S1). As shown in Figure 2b, the average thickness of the NPL increased from 3.89 to 4.13 nm as the ratio of Cs to Pb was increased. A PL emission near 460 nm is known to be 3 monolayers (ML) thick of CsPbBr₃ IPNPLs.³³ The increase in average thickness is due to the increase of NPLs thicker than 3 ML thick. Some spectra are observed at the 490–500 nm peak, known as PL emission of 6 ML thick CsPbBr₃ IPNPL (Figure 2a,d,2e).³³ This is because NPLs with a thickness of 3 ML were agglomerated to form 6 ML thick NPLs. So, our NPLs have 2 peaks in thickness distribution (Figure S2). Therefore, the average thickness increased and a red shift occurred (Figure 2a,b). In addition, as the amount of cesium increases, the growth of the NPL accelerates.³⁴ The NPLs grow faster due to the increased rate of cesium ions to oleylammonium ions, which occupy the A site of the perovskite structure.³⁴ As a result, the overall average thickness became thicker, resulting in a red shift (Figure 2a,2b).

We performed XRD analyses to clarify the shapes of the nanocrystals, as shown in Figure 2c. Based on the XRD results, we confirmed that the diffraction patterns were the same as those for the bulk CsPbBr₃ structure, but the peak intensities were different. The intensities of peaks for the (100) and (200) planes were greater than those for the other planes. This was because the nanocrystals grew into one plane and became NPLs.³⁵ Additionally, Figure 2c shows that the intensities of all of the peaks except those for the (100) and (200) planes increased as the ratio of Cs to Pb increased. As the thicknesses of the NPLs increased, the intensities for the other plane directions increased. Therefore, we concluded that we controlled the thickness of the NPLs by adjusting the Cs-to-Pb ratio.

An additional peak, not in the CsPbBr₃ pattern, was observed at 12.48° (Figure 2c). This peak was also not observed in the patterns of CsBr, PbBr₂, Cs₄PbBr₆, CsPb₂Br₅, or any other phases of compounds with cesium, lead, and bromide. If the NPLs were stacked over a regular distance, XRD patterns were observed (Figure S3).^{35,36} Therefore, we measured the XRD pattern from a lower angle to confirm the stacked NPL peaks. The measured peaks were at 5.38, 7.09, 8.85, 10.78, and 12.48°, except for the CsPbBr₃ peaks (Figure S4). The average distance of our NPLs was measured to be 4.97 nm, and we calculated the 2-theta distance with this value by Bragg's law (eq 1). The calculated 2-theta values and the measured values were almost the same (Table S6). Therefore, we confirmed that the peak at 12.48° is a stacked NPL peak.

$$n\lambda = 2d \sin \theta \quad (1)$$

Controlling Ligands. NPLs have larger surface-to-volume ratios than general nanocrystals, so more ligands are commonly used on the surface.²⁴ Because of the large surface, the ligands have a more significant effect on NPL synthesis than general nanocrystals.²⁴ In this study, we adjusted the amounts of ligands used to find the optimal conditions for synthesizing NPLs. First, we controlled the amount of oleic acid used and analyzed the extent of synthesis by measuring the PL intensity. The peak position blue-shifted as the amount of oleic acid was increased (Figure 2d), and the nanoparticle syntheses did not proceed well except in the cases involving 2.0 and 2.5 mL of oleic acid. Similarly, as the amount of oleylamine was increased, the PL peak positions corresponding to the synthesized NPLs blue-shifted (Figure 2e). However, multiple peaks appeared when too much oleylamine was added.

As the amount of ligand that formed the surfaces of the NPLs increased, the surface-to-volume ratio increased, resulting in thinner and smaller NPLs.³¹ Accordingly, blue shifts occurred with increasing amounts of ligand added (Figure 2d,2e). As the oleic acid concentration increased, the nanocrystal sizes decreased (Figure 2f). In addition, we confirmed that the thicknesses of the NPLs decreased when the amount of oleylamine used was increased (Figure 2g). When 0.8, 0.9, or 1.0 mL of oleylamine was added, the average thickness of the nanoplatelets was 4.17, 4.03, or 3.75 nm, respectively (Figure S5). The NPL thickness becomes thinner as the amount of oleylamine increases because the A site of the perovskite structure is occupied by oleylammonium ion instead of cesium ion, making it difficult to grow nanoparticles.³⁴ When we adjusted the amount of oleic acid, the concentration in the synthetic solution was deficient. The only synthesis that proceeded well was that with 2.0 mL (Figure 2h). Therefore, we confirmed with XRD that most NPLs were transformed to CsPb₂Br₅ during the washing process (Figure 2h). The peak at 11.6° was attributed to the CsPb₂Br₅ structure, which appeared to form when the ligands were removed from the nanoplatelet structure. To confirm this, we analyzed the XRD data as a function of the washing process used to remove the ligand. As shown in Figure S6, as washing was repeated, the position of the XRD peak shifted to 11.6°. In general, when the amount of lead was increased or that of cesium was decreased in the CsPbBr₃ structure, the structure transformed into a CsPb₂Br₅ structure.³⁷ In the case of NPLs, since many ligands were included in place of cesium ion in the A sites, when the ligand was removed, it was as if the A site ion was removed, and the structure was transformed into a CsPb₂Br₅ structure.³⁷ We washed the solution to remove ligands on the surfaces of the NPLs. Accordingly, the $L_2[ABX_3]_{n-1}BX_4$ structure was stoichiometrically transformed into an AB₂X₅ structure, which shifted the XRD peak to 11.6° (Figure S6). We washed the NPLs 1–3 times and confirmed that the XRD peak at 11.6° remained after 3 washes. This indicated that when the ligands on the surface were removed, the NPL structure was transformed into a CsPb₂Br₅ structure.

When the amount of oleylamine added was adjusted within the range of 0.8–1.4 mL, as shown in Figure 2g, NPLs were synthesized with oleylamine volumes ranging from 0.8 to 1.0 mL. Using XRD analyses, we confirmed that the relative intensity of the (100) peak increased as the amount of oleylamine increased (Figure 2i). However, when the amount of ligand was increased too much, the nanocrystals became very small, and it was difficult to grow NPLs because the ions were encapsulated by the ligands (Tables S2 and S3).

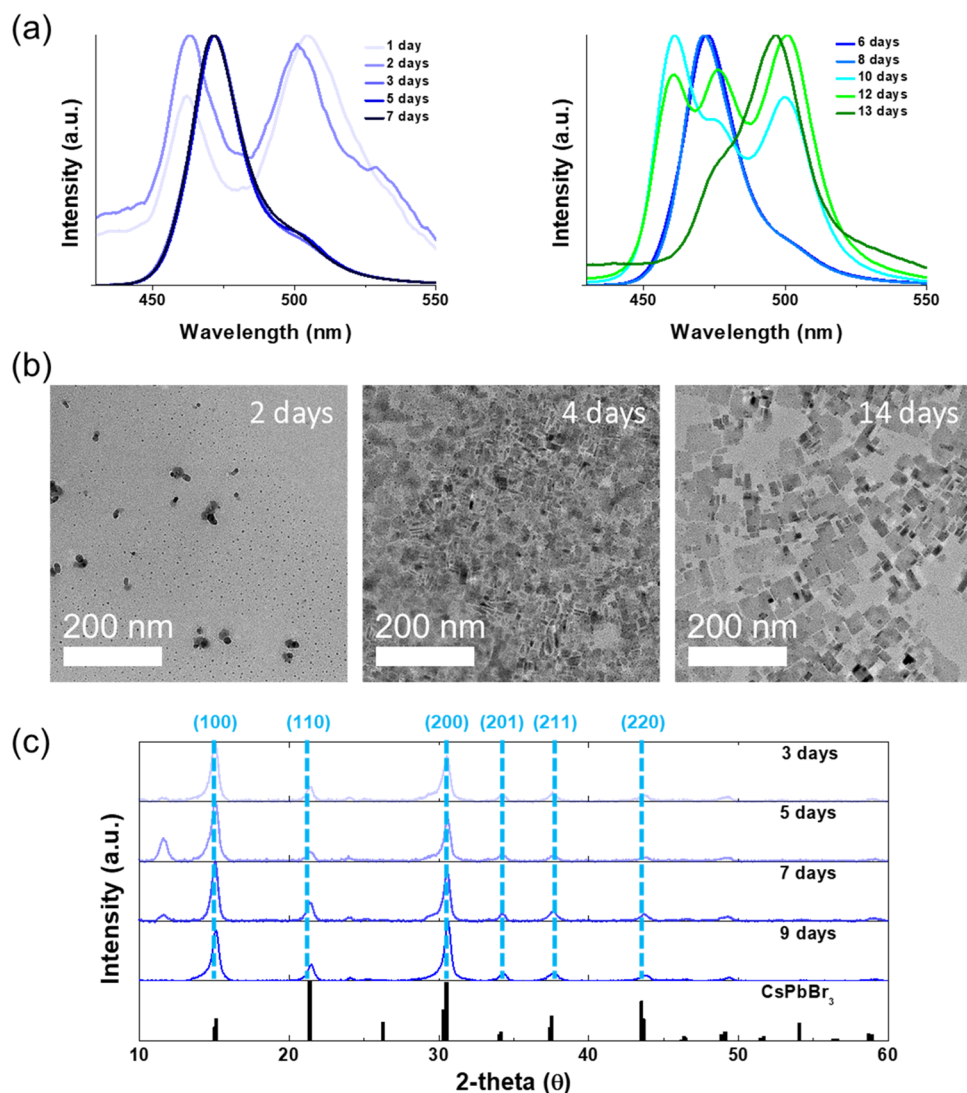


Figure 3. (a) PL spectra before 7 days (left) and after 6 days (right) of synthesis time, (b) TEM images for NPLs growth during synthesis time, and (c) XRD patterns for NPLs with different synthesis times.

Controlling the Solubility with DMSO. A small amount of DMSO was added to ionize CsBr and PbBr₂.¹ The solubilities of the ions depended on the amount of DMSO used, so we controlled the synthesis rate by adding DMSO. However, if too much DMSO was added, nanosize particles could not be formed, and Ostwald ripening was accelerated, leaving only large particles.³⁸

If the amount of DMSO used was too small, the synthesis time increased and so the cost increased. Therefore, to analyze the effects, we ran the reactions for a certain amount of time according to the amount of DMSO used. We varied the amount of DMSO in 20 μL increments and ran the reactions for 72 h. The PL intensities are shown in Figure 2j.

As the amount of DMSO added was increased, a blue shift occurred, and when more than 180 μL was added, a red shift occurred; and when the concentration was very low, most of the NPLs had disappeared (Figure 2j). The samples with 20–60 μL of DMSO added were still undergoing synthesis because the rates were low. When 80–160 μL was added, there were no significant differences in the PL peak positions, and it was confirmed that the absorption peaks and PL spectra were similar (Figure 2k). Accordingly, although the synthesis rates

differed depending on the amount of DMSO used, it was confirmed that there was no significant difference in PL performance from the time at which the NPLs were synthesized until they disappeared due to Ostwald ripening.³⁸

Effects of Synthesis Time on NPLs. To analyze the NPL synthesis, we controlled the synthesis times, while other conditions remained fixed. The PL spectra obtained at different times after synthesis are shown in Figure 3a. Constant PL peak positions were observed from 3 days after synthesis to 8 days; we confirmed that a peak appeared at 500 nm after 9 days, and then multiple peaks gradually appeared after that. Finally, we confirmed that the PL peak had moved to 500 nm on day 13 after synthesis. This red shift of the PL peak was caused by the growth of the NPLs.²⁰ As shown in Figure 3b, we confirmed that NPLs did not form until 2 days after the synthesis began and the product existed in the form of small particles. In the TEM image obtained 4 days after synthesis, we observed that NPLs were formed, and in the TEM image obtained 14 days after synthesis, we confirmed that the NPLs had grown very large (Figure 3b). We performed XRD analyses to confirm the growth of NPLs for each time period (Figure 3c). The XRD patterns of the samples could not be

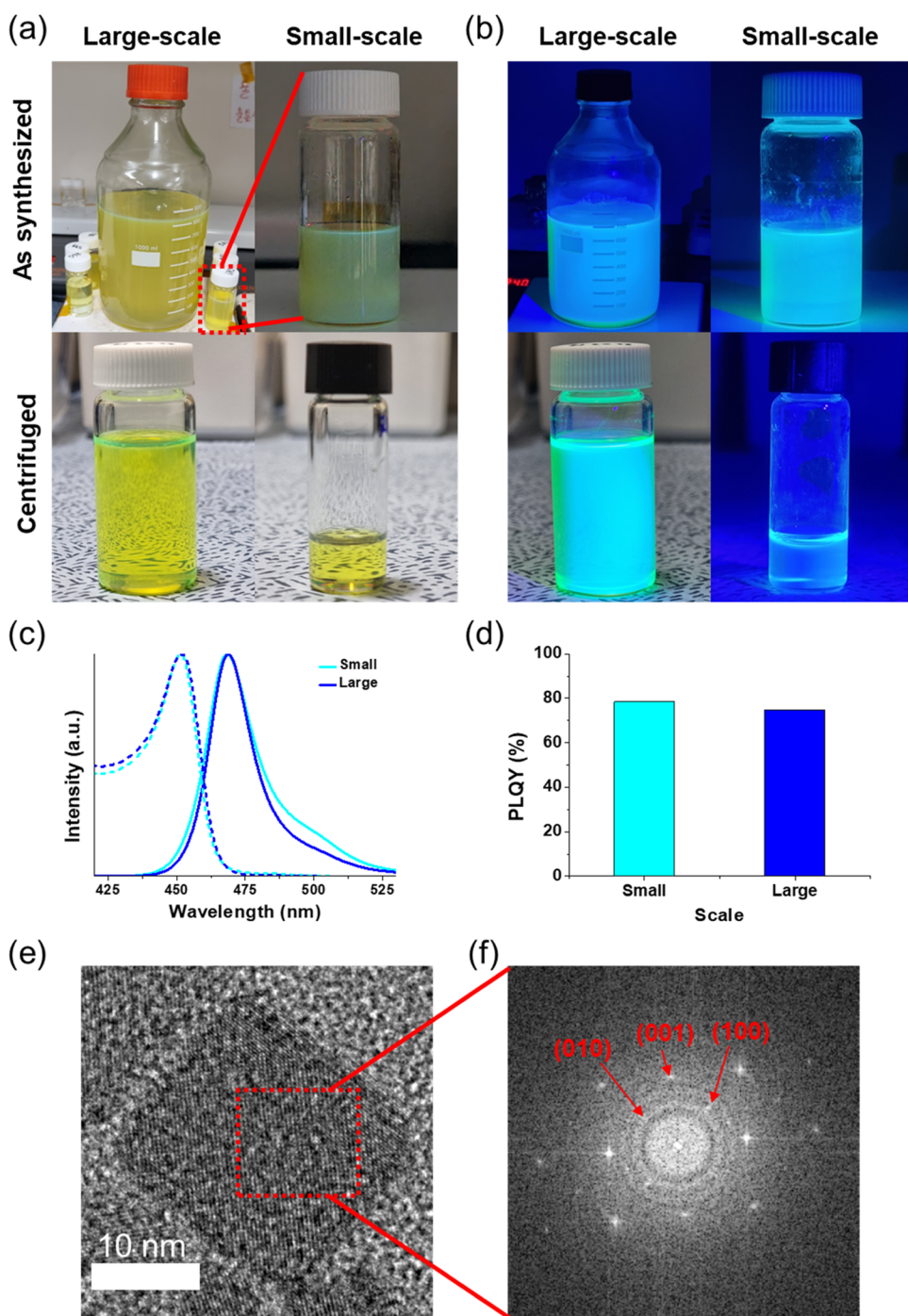


Figure 4. Images of large- and small-scale NPL solutions (a) under ambient light and (b) with UV illumination. (c) Comparison of PL (solid lines) and UV-vis absorption (dashed lines) spectra for large- and small-scale NPL solutions. (d) PLQY comparison of blue IPNCs prepared by large-scale and small-scale syntheses. (e) TEM image of an IPNC made using a large-scale synthesis and (f) its corresponding FFT pattern for the selected area.

analyzed, except those that were synthesized between 3 and 9 days because of low concentrations. There were no differences in the positions of the peaks according to the synthesis times, and the peak positions appeared to be the same as those observed in the diffraction pattern for bulk CsPbBr_3 . However, the intensities of the (100) and (200) peaks were very high because of the anisotropic shapes of the NPLs. We confirmed that the intensity of the (100) peak decreased after 9 days because the NPLs began to thicken. The stacked NPL XRD peak at 12.48° was observed. This peak increased until day 5

and then decreased. The concentration of the NPL solution caused a change in the peak intensity. The number of NPLs increased until day 5 because the synthesis was continued. After day 5, the number of nanoplatelets decreased because the nanoplatelets aggregated to a large size.

Large-Scale Synthesis. For large-scale synthesis, 60 times the amount used for small-scale synthesis was employed. All other synthetic conditions were the same, and a 1 L bottle was used instead of a 20 mL vial. Since the synthesis rate was controlled so that the synthesis method was not affected by the

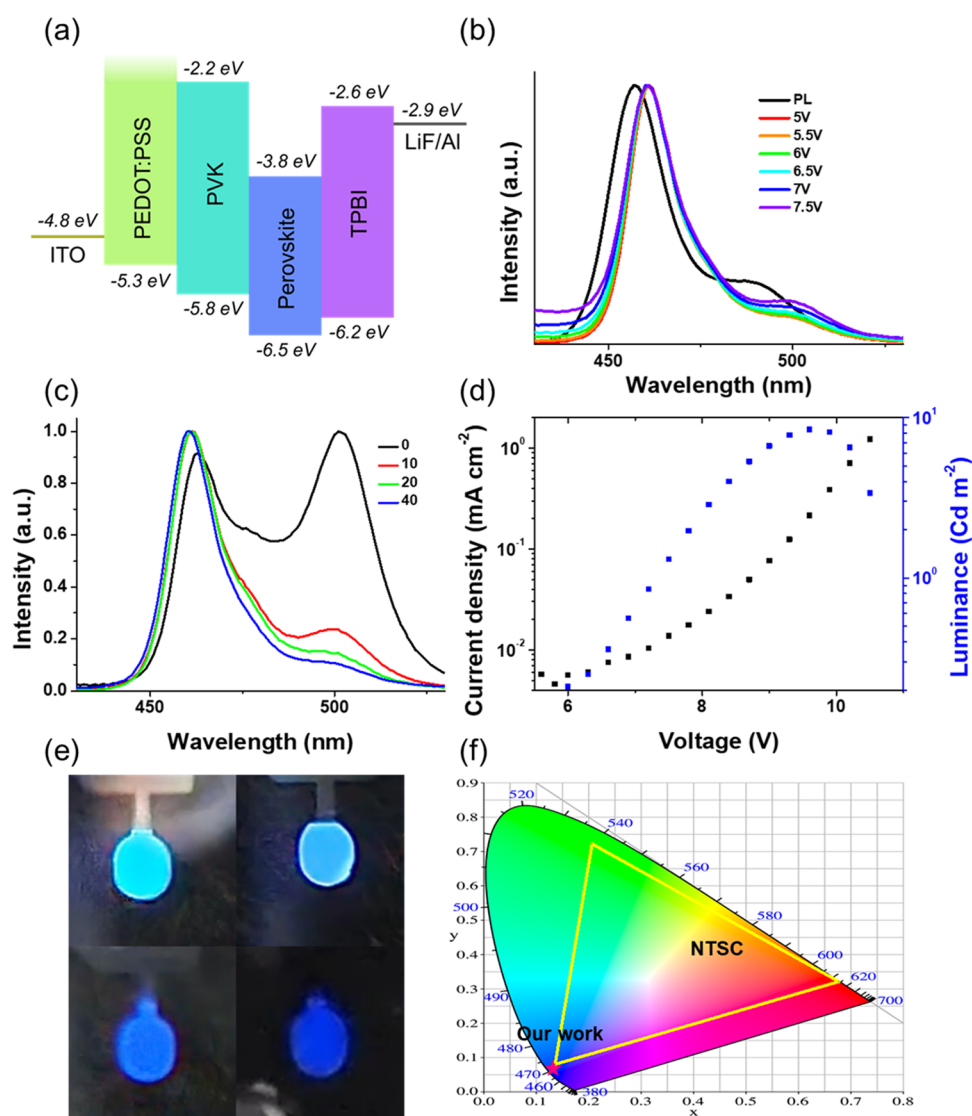


Figure 5. (a) Energy diagrams for the NPL-based blue LEDs. (b) EL spectra of the PeLED by the applied voltage and PL spectrum of the NPL solution. (c) EL spectra under 6 V voltage of LEDs according to the amount of post-treatment ZnBr_2 solution (concentration of ZnBr_2 solution, 0, 10, 20, and 40 $\mu\text{L}/\text{mL}$). (d) J - V - L curve for the NPL-based LED (black squares indicate current density, and blue squares indicate the luminance). (e) Images of blue LEDs using large-scale synthesized NPLs with 460 to 470 nm electroluminescence peaks. (f) CIE color coordinates corresponding to NPLs and NTSC standards.

size of the container, the synthesis of NPLs exhibiting consistent performance was possible. As shown in Figure 4a,4b, we confirmed that blue PL resulted regardless of the size of the container. Although the colors appearing in Figure 4b seem to be slightly different depending on the camera conditions and the surrounding environment, it was confirmed that there was no difference in the PL measurement results (Figure 4c). Rather, as shown in Figure 4c, the fwhm was narrower for large-scale synthesis. In the case of large-scale synthesis, the errors in the amounts of compounds added were less significant than those during the small-scale synthesis, so a more consistent performance was possible at this scale. We confirmed that the PL spectra and absorption spectra for NPLs prepared via large- and small-scale syntheses are almost identical, so there was no difference in the properties of NPLs. Therefore, it was easy to adjust the desired synthetic conditions for small-scale synthesis and apply them directly to large-scale synthesis. Additionally, the PLQYs of NPLs prepared by small-scale and large-scale synthesis showed a

difference of less than 4%, confirming that the amount synthesized did not affect the NPL quality. As shown in Figure 4e,4f, we confirmed that NPLs synthesized on a large scale also possessed a CsPbBr_3 structure.

Fabrication of Blue LEDs. An LED device with a multilayer structure consisting of ITO, poly(2,3-dihydrothieno-1,4-dioxin)-poly(styrenesulfonate) (PEDOT:PSS), CsPbBr_3 IPNPLs, 2,2',2''-(1,3,5-benzinetriyl)-tris(1-phenyl-1-H-benzimidazole) (TPBI), LiF, and Al was fabricated, in which CsPbBr_3 IPNPLs were used as the emitting layer (Figure 5a). The NPLs were treated with ethyl acetate once in the PL measurement, but we could not fabricate light-emitting diodes with them due to excess ligands. Therefore, ethyl acetate treatment was performed twice to remove the excess ligands and post-treatment with ZnBr_2 was used to fabricate light-emitting diodes. There was no significant difference in the PL properties of the NPLs washed with ethyl acetate once and of the post-treated NPLs after washing twice with ethyl acetate (Figure S7). As plotted in Figure 5b, a sharp peak at 461 nm

was detected in the EL emission spectrum, with an fwhm of 17 nm. We obtain an EQE of 0.233% for blue PeLEDs (Figures S8 and S9). A 4 nm red shift of the EL peak was observed compared to the PL peak for NPLs (Figure 5b). A red shift did not occur during LED operation and voltage rise because only bromide ions were used (Figure 5b). In addition, we confirmed that red-shift did not occur when comparing the EL spectra of LEDs and the PL spectrum of the thin film (Figure S10). Although the surface of the NPL thin film was analyzed by SEM and AFM images, it was difficult to observe the particles affected by the ligands, and the roughness of the film surface was measured at 1.606 nm (Figures S11 and S12).

We fabricated NPL-embedded polymer films with polystyrene-*block*-poly(ethylene-*ran*-butylene)-*block*-polystyrene (SEBS). We confirmed that these films were stable in ambient conditions (Figure S13). The PLQY of polymer film is similar to the NPL solution, about 82.5% (Figure S14).

When PeLEDs were fabricated, the NPL solution was post-treated with ZnBr₂ solution to remove defects. As the amount of ZnBr₂ solution increased, we confirmed that the 490–500 nm peak intensity decreased (Figure 5c). However, as the amount of ZnBr₂ solution increased, the electrical conductivity decreased because oleylamine increased (Figure S15). Therefore, the most optimal post-treatment solution condition was to add the ZnBr₂ solution to the NPL solution at a concentration of 20 μL/mL (Figure 5d).

By comparing the 500 nm peak of the LED with the PL of the NPL solution, we confirmed that the large particles were not entirely removed during centrifugation. Complete removal of the 500 nm particles could result in a blue LED emitting at 460 nm. In addition, we confirmed that when nanoparticles of different emitting wavelengths coexisted, nanoparticles could emit each wavelength rather than mix. Anion exchange did not occur because CsPbBr_{3-x}Cl_x, in which halogen ions were mixed, was not used. Since ion migration did not occur, phase separation did not occur, and no red shift of the peak was observed. As shown in Figure 5e, we observed that the LED emitted blue light. The brightness of the LED was low, which was improved when we adjusted each layer of the LEDs. Figure 5f shows the CIE color coordinates, and we confirmed that the PeLED emitted a color outside of the National Television Standard Committee (NTSC) color triangle. We observed a sharp blue color upon removing the nanoparticles emitting at 500 nm. In this work, because only CsPbBr₃ IPNPLs were used, no anion exchange could occur, which may pave the way for practical applications of blue LEDs and mixed wavelength PeLEDs.

CONCLUSIONS

In this study, we developed a room-temperature, one-pot synthetic method. Unlike previous synthesis methods, our developed method was performed in homogeneous solutions by increasing the reaction time. Even though we increased the synthetic scale with this method, the synthesized nanoparticles were uniform and exhibited a PL peak at 460 nm, a PLQY of 78%, an fwhm of 18 nm, and particle thicknesses of 2.88 nm. In our new IPNPL synthesis method, variables such as Cs-to-Pb ratio, amount of ligands, amount of DMSO, and synthesis time were adjusted. We confirmed that the thickness of the nanoplatelet synthesized by each variable changes, and as the thickness becomes thinner, the emission peak shows a blue shift due to the quantum confinement effect becoming larger. Large-scale synthesis was possible, and it was possible to

perform the synthesis at room temperature under an ambient atmosphere, which improved productivity. When the system was fabricated with LEDs, an EL peak at 461 nm and an fwhm of 17 nm were measured. It seems that the PLQY and EL can be improved through post-treatment, the ligand process, or optimization of the emitting layer thickness. This study will greatly facilitate the commercialization of IPNCs.

METHODS

Materials. Cesium bromide (CsBr, 99.999%), lead bromide (PbBr₂, 99.999%), oleic acid (OA, 90%), oleylamine (OAm, 70%), ethyl acetate (99.8%), poly(9-vinylcarbazole) (PVK, *M_n* 25,000–50,000), chlorobenzene (99.8%), and polystyrene-*block*-poly(ethylene-*ran*-butylene)-*block*-polystyrene (SEBS) were purchased from Sigma-Aldrich. Toluene, acetone, isopropyl alcohol (IPA), and dimethyl sulfoxide (DMSO) were purchased from Duksan Pure Chemical. Poly(2,3-dihydrothieno-1,4-dioxin)-poly(styrenesulfonate) (PEDOT:PSS, AI 4083) was purchased from Heraeus.

Synthesis of Nanoplatelets. A total of 0.32 mmol of CsBr and 0.4 mmol of PbBr₂ were loaded into a 20 mL vial, and 10 mL of toluene, 2 mL of OA, 0.9 mL of OAm, and 100 μL of DMSO were added. After that, the solution was stirred at 300 rpm and room temperature for 72 h. At the end of stirring, the solution was centrifuged in two steps to separate the NPLs. First, the obtained solution was centrifuged at 12,000 rpm for 5 min to remove the large particles. The precipitate was discarded, and ethyl acetate was added in a 1:2 ratio to the supernatant. Then, the NPLs in solution were centrifuged at 12,000 rpm for 5 min to remove the ligands, DMSO, and unreacted chemicals. The precipitate was collected and redispersed in toluene. Then, ethyl acetate was added in a 1:3 ratio to the solution. The mixed solution was centrifuged at 12,000 rpm for 5 min to wash out the ligands. The precipitate was collected and redispersed in hexane.

Large-Scale Synthesis of Nanoplatelets. Large-scale synthesis was performed by increasing the amounts of precursors used in the small-scale synthesis. A total of 19.2 mmol of CsBr and 24 mmol of PbBr₂ were loaded into a 1 L bottle, and 600 mL of toluene, 120 mL of OA, 54 mL of OA, and 6 mL of DMSO were added. After that, the solution was stirred at 300 rpm at room temperature for 72 h. At the end of stirring, the solution was centrifuged in two steps to separate the NPLs. First, the obtained solution was centrifuged at 12,000 rpm for 5 min to remove the large particles. The precipitate was discarded, and ethyl acetate was added at a 1:2 ratio to the supernatant. Then, the NPLs in solution were centrifuged at 12,000 rpm for 5 min to remove the ligands, DMSO, and unreacted chemicals. The precipitate was collected and redispersed in toluene. Then, ethyl acetate was added in a 1:3 ratio to the solution. The mixed solution was centrifuged at 12,000 rpm for 5 min to wash out the ligands. The precipitate was collected and redispersed in hexane.

ZnBr₂ Posttreatment. ZnBr₂ (0.3 mmol) was loaded into a vial, and 10 mL of hexane and 0.2 mL of aqueous OAm were added. After that, the solution was stirred at 300 rpm for 24 h. We added 40 μL of the ZnBr₂ solution to 1 mL of the synthesized NPL solution.

Device Fabrication. A 2.5 cm × 2.5 cm glass was washed via sequential ultrasonication in acetone, IPA, and deionized water for 5 min each. Patterned ITO with a thickness of 100 nm was deposited on the glass using a direct current magnetron sputter. The ITO-deposited glass was oxygen plasma-treated at 140 W for 90 s. On the ITO-deposited glass, the HTL solution (1:1 PEDOT:PSS and isopropyl alcohol) was spin-coated at 4000 rpm for 60 s and annealed at 130 °C for 20 min. Then, PVK solution (10 mg/mL, chlorobenzene) was spin-coated at 2000 rpm for 30 s on the HTL in a nitrogen-filled glovebox and annealed at 120 °C for 10 min. The obtained NPL solution was spin-coated at 2000 rpm for 60 s in a nitrogen-filled glovebox. A 45 nm thick TPBi layer, a 1 nm thick LiF layer, and a 100 nm thick Al layer were sequentially deposited on the emitting layer using a thermal evaporator.

Polymer Film Fabrication. SEBS (1.5 g) was loaded in the vial, and NPL solution (8.5 g) redispersed in toluene was added. The

solution was stirred at 300 rpm at room temperature for 2 h. The polymer solution was coated on a glass substrate and dried at room temperature for 3 h.

Characterization. PL emission spectra and PLQYs were collected with a Jasco FP-8500 spectrofluorometer. Absorption spectra were measured with a UV-vis spectrometer. TEM images were obtained with a JEM-ARM 200F NEOARM (JEOL). XRD measurements were performed with a SmartLab system (Rigaku). The EL spectrum of the device was measured by using a spectroradiometer (Konica, CS 2000).

■ ASSOCIATED CONTENT

SI Supporting Information

The Supporting Information is available free of charge at <https://pubs.acs.org/doi/10.1021/acsami.3c03139>.

PL properties of synthesized NPLs according to each variable; additional TEM, XRD, and PL spectra data; and explanation of stacked NPLs making additional XRD peaks (PDF)

■ AUTHOR INFORMATION

Corresponding Author

Jin-Woo Park – Department of Materials Science and Engineering, Yonsei University, Seoul 03722, Republic of Korea; orcid.org/0000-0003-0965-373X; Phone: +82-221235834; Email: jwpark09@yonsei.ac.kr; Fax: +82-221235834

Authors

Ju-Hyun Yoo – Department of Materials Science and Engineering, Yonsei University, Seoul 03722, Republic of Korea

Sungjin Kim – Department of Materials Science and Engineering, Seoul National University, Seoul 08826, Republic of Korea

Hyeokjung Lee – Department of Materials Science and Engineering, Yonsei University, Seoul 03722, Republic of Korea

Cheolmin Park – Department of Materials Science and Engineering, Yonsei University, Seoul 03722, Republic of Korea; orcid.org/0000-0002-6832-0284

Tae-Woo Lee – Department of Materials Science and Engineering, Seoul National University, Seoul 08826, Republic of Korea; School of Chemical and Biological Engineering, Institute of Engineering Research, Research Institute of Advanced Materials, Soft Foundry, Seoul National University, Seoul 08826, Republic of Korea; orcid.org/0000-0002-6449-6725

Complete contact information is available at: <https://pubs.acs.org/doi/10.1021/acsami.3c03139>

Notes

The authors declare no competing financial interest.

■ ACKNOWLEDGMENTS

This work was supported by a National Research Foundation of Korea (NRF) grant funded by the Korean government (MSIT) (no. 2021R1A2C2004297) and a National Research Foundation of Korea (NRF) grant funded by the Korean government (MSIT) (no. NRF-2021R1A4A1032129).

■ REFERENCES

- (1) Li, X.; Wu, Y.; Zhang, S.; Cai, B.; Gu, Y.; Song, J.; Zeng, H. CsPbX₃ Quantum Dots for Lighting and Displays: Room-Temperature Synthesis, Photoluminescence Superiorities, Underlying Origins and White Light-Emitting Diodes. *Adv. Funct. Mater.* **2016**, *26* (15), 2435–2445.
- (2) Li, J.; Xu, L.; Wang, T.; Song, J.; Chen, J.; Xue, J.; Dong, Y.; Cai, B.; Shan, Q.; Han, B. 50-Fold EQE Improvement up to 6.27% of Solution-Processed All-Inorganic Perovskite CsPbBr₃ QLEDs via Surface Ligand Density Control. *Adv. Mater.* **2017**, *29* (5), No. 1603885.
- (3) Wei, Y.; Cheng, Z.; Lin, J. An Overview on Enhancing the Stability of Lead Halide Perovskite Quantum Dots and Their Applications in Phosphor-Converted LEDs. *Chem. Soc. Rev.* **2019**, *48* (1), 310–350.
- (4) Zhang, C.; Wang, B.; Zheng, W.; Huang, S.; Kong, L.; Li, Z.; He, G.; Li, L. Hydrofluoroethers as Orthogonal Solvents for All-Solution Processed Perovskite Quantum-Dot Light-Emitting Diodes. *Nano Energy* **2018**, *51*, 358–365.
- (5) Kovalenko, M. V.; Protesescu, L.; Bodnarchuk, M. I. Properties and Potential Optoelectronic Applications of Lead Halide Perovskite Nanocrystals. *Science* **2017**, *358* (6364), 745–750.
- (6) Oh, J. W.; Han, H.; Kim, H. H.; Lee, H.; Kim, D.; Lee, J.; Kim, J.; Choi, W. K.; Park, C. Metal–Organic Framework-Assisted Metal-Ion Doping in All-Inorganic Perovskite for Dual-Mode Image Sensing Display. *Adv. Funct. Mater.* **2022**, *32* (18), No. 2111894.
- (7) Kim, T.; Kim, J.-H.; Park, J.-W. Semi-Transparent Organic-Inorganic Hybrid Perovskite Light-Emitting Diodes Fabricated under High Relative Humidity. *Solid-State Electron.* **2020**, *165*, No. 107749.
- (8) Kim, Y.-H.; Kim, S.; Kakekhani, A.; Park, J.; Park, J.; Lee, Y.-H.; Xu, H.; Nagane, S.; Wexler, R. B.; Kim, D.-H.; et al. Comprehensive Defect Suppression in Perovskite Nanocrystals for High-Efficiency Light-Emitting Diodes. *Nat. Photonics* **2021**, *15* (2), 148–155.
- (9) Zhou, C.; Lin, H.; He, Q.; Xu, L.; Worku, M.; Chaaban, M.; Lee, S.; Shi, X.; Du, M.-H.; Ma, B. Low Dimensional Metal Halide Perovskites and Hybrids. *Mater. Sci. Eng., R* **2019**, *137*, 38–65.
- (10) Chen, G.; Lin, W.; Chen, H.; Guo, T. Ultra-High Stability of Cesium Lead Halide Nanocrystals Synthesized by a Simple One-Pot Method. *Mater. Des.* **2019**, *181*, No. 108100.
- (11) Sun, S.; Yuan, D.; Xu, Y.; Wang, A.; Deng, Z. Ligand-Mediated Synthesis of Shape-Controlled Cesium Lead Halide Perovskite Nanocrystals via Reprecipitation Process at Room Temperature. *ACS Nano* **2016**, *10* (3), 3648–3657.
- (12) Quan, L. N.; Garcia de Arquer, F. P.; Sabatini, R. P.; Sargent, E. H. Perovskites for Light Emission. *Adv. Mater.* **2018**, *30* (45), No. 1801996.
- (13) Sichert, J. A.; Tong, Y.; Mutz, N.; Vollmer, M.; Fischer, S.; Milowska, K. Z.; Garcia Cortadella, R.; Nickel, B.; Cardenas-Daw, C.; Stolarczyk, J. K.; et al. Quantum Size Effect in Organometal Halide Perovskite Nanoplatelets. *Nano Lett.* **2015**, *15* (10), 6521–6527.
- (14) Wang, Y.-K.; Singh, K.; Li, J.-Y.; Dong, Y.; Wang, X.-Q.; Pina, J. M.; Yu, Y.-J.; Sabatini, R.; Liu, Y.; Ma, D.; et al. In Situ Inorganic Ligand Replenishment Enables Bandgap Stability in Mixed-Halide Perovskite Quantum Dot Solids. *Adv. Mater.* **2022**, *34* (21), No. 2200854.
- (15) Dong, Y.; Wang, Y. K.; Yuan, F.; Johnston, A.; Liu, Y.; Ma, D.; Choi, M. J.; Chen, B.; Chekini, M.; Baek, S. W.; et al. Bipolar-Shell Resurfacing for Blue LEDs Based on Strongly Confined Perovskite Quantum Dots. *Nat. Nanotechnol.* **2020**, *15* (8), 668–674.
- (16) Vashishtha, P.; Ng, M.; Shivarudraiah, S. B.; Halpert, J. E. High Efficiency Blue and Green Light-Emitting Diodes Using Ruddlesden–Popper Inorganic Mixed Halide Perovskites with Butylammonium Interlayers. *Chem. Mater.* **2019**, *31* (1), 83–89.
- (17) Bohn, B. J.; Tong, Y.; Gramlich, M.; Lai, M. L.; Doblinger, M.; Wang, K.; Hoyer, R. L. Z.; Muller-Buschbaum, P.; Stranks, S. D.; Urban, A. S.; et al. Boosting Tunable Blue Luminescence of Halide Perovskite Nanoplatelets through Postsynthetic Surface Trap Repair. *Nano Lett.* **2018**, *18* (8), 5231–5238.

- (18) Yin, W.; Li, M.; Dong, W.; Luo, Z.; Li, Y.; Qian, J.; Zhang, J.; Zhang, W.; Zhang, Y.; Kershaw, S. V.; et al. Multidentate Ligand Polyethylenimine Enables Bright Color-Saturated Blue Light-Emitting Diodes Based on CsPbBr₃ Nanoplatelets. *ACS Energy Lett.* **2021**, *6* (2), 477–484.
- (19) Jiang, Y.; Sun, C.; Xu, J.; Li, S.; Cui, M.; Fu, X.; Liu, Y.; Liu, Y.; Wan, H.; Wei, K.; et al. Synthesis-on-substrate of quantum dot solids. *Nature* **2022**, *612* (7941), 679–684.
- (20) Singldinger, A.; Gramlich, M.; Gruber, C.; Lampe, C.; Urban, A. S. Nonradiative Energy Transfer between Thickness-Controlled Halide Perovskite Nanoplatelets. *ACS Energy Lett.* **2020**, *5* (5), 1380–1385.
- (21) Jang, H. M.; Park, J.; Kim, S.; Lee, T.-W. Quantum-Confinement Effect on the Linewidth Broadening of Metal Halide Perovskite-Based Quantum Dots. *J. Phys.: Condens. Matter* **2021**, *33* (35), No. 355702.
- (22) Protesescu, L.; Yakunin, S.; Bodnarchuk, M. I.; Krieg, F.; Caputo, R.; Hendon, C. H.; Yang, R. X.; Walsh, A.; Kovalenko, M. V. Nanocrystals of Cesium Lead Halide Perovskites (CsPbX₃, X = Cl, Br, and I): Novel Optoelectronic Materials Showing Bright Emission with Wide Color Gamut. *Nano Lett.* **2015**, *15* (6), 3692–3696.
- (23) Liu, X.-K.; Xu, W.; Bai, S.; Jin, Y.; Wang, J.; Friend, R. H.; Gao, F. Metal halide perovskites for light-emitting diodes. *Nat. Mater.* **2021**, *20* (1), 10–21.
- (24) Peng, S.; Wang, S.; Zhao, D.; Li, X.; Liang, C.; Xia, J.; Zhang, T.; Xing, G.; Tang, Z. Pure Bromide-Based Perovskite Nanoplatelets for Blue Light-Emitting Diodes. *Small Methods* **2019**, *3* (10), No. 1900196.
- (25) Zhang, F.; Zhong, H.; Chen, C.; Wu, X.-g.; Hu, X.; Huang, H.; Han, J.; Zou, B.; Dong, Y. Brightly Luminescent and Color-Tunable Colloidal CH₃NH₃PbX₃ (X = Br, I, Cl) Quantum Dots: Potential Alternatives for Display Technology. *ACS Nano* **2015**, *9* (4), 4533–4542.
- (26) Nedelcu, G.; Protesescu, L.; Yakunin, S.; Bodnarchuk, M. I.; Grotevent, M. J.; Kovalenko, M. V. Fast Anion-Exchange in Highly Luminescent Nanocrystals of Cesium Lead Halide Perovskites (CsPbX₃, X = Cl, Br, I). *Nano Lett.* **2015**, *15* (8), 5635–5640.
- (27) Akkerman, Q. A.; D’Innocenzo, V.; Accornero, S.; Scarpellini, A.; Petrozza, A.; Prato, M.; Manna, L. Tuning the Optical Properties of Cesium Lead Halide Perovskite Nanocrystals by Anion Exchange Reactions. *J. Am. Chem. Soc.* **2015**, *137* (32), 10276–10281.
- (28) Wei, S.; Yang, Y.; Kang, X.; Wang, L.; Huang, L.; Pan, D. Room-Temperature and Gram-Scale Synthesis of CsPbX₃ (X = Cl, Br, I) Perovskite Nanocrystals with 50–85% Photoluminescence Quantum Yields. *Chem. Commun.* **2016**, *52* (45), 7265–7268.
- (29) Kumawat, N. K.; Liu, X.-K.; Kabra, D.; Gao, F. Blue Perovskite Light-Emitting Diodes: Progress, Challenges and Future Directions. *Nanoscale* **2019**, *11* (5), 2109–2120.
- (30) Lan, J.; Luo, L.; Wang, M.; Li, F.; Wu, X.; Wang, F. One Pot Gram-Scale Synthesis of CsPbBr₃ Nanocrystals and Their Application in Green LED. *J. Lumin.* **2019**, *210*, 464–471.
- (31) Cho, J.; Choi, Y.-H.; O’Loughlin, T. E.; De Jesus, L.; Banerjee, S. Ligand-Mediated Modulation of Layer Thicknesses of Perovskite Methylammonium Lead Bromide Nanoplatelets. *Chem. Mater.* **2016**, *28* (19), 6909–6916.
- (32) Weidman, M. C.; Goodman, A. J.; Tisdale, W. A. Colloidal Halide Perovskite Nanoplatelets: An Exciting New Class of Semiconductor Nanomaterials. *Chem. Mater.* **2017**, *29* (12), 5019–5030.
- (33) Otero-Martínez, C.; Ye, J.; Sung, J.; Pastoriza-Santos, I.; Pérez-Juste, J.; Xia, Z.; Rao, A.; Hoyer, R. L. Z.; Polavarapu, L. Colloidal Metal-Halide Perovskite Nanoplatelets: Thickness-Controlled Synthesis, Properties, and Application in Light-Emitting Diodes. *Adv. Mater.* **2022**, *34* (10), No. 2107105.
- (34) Antami, K.; Bateni, F.; Ramezani, M.; Hauke, C. E.; Castellano, F. N.; Abolhasani, M. CsPbI₃ Nanocrystals Go with the Flow: From Formation Mechanism to Continuous Nanomanufacturing. *Adv. Funct. Mater.* **2022**, *32* (6), No. 2108687.
- (35) Akkerman, Q. A.; Motti, S. G.; Srimath Kandada, A. R.; Mosconi, E.; D’Innocenzo, V.; Bertoni, G.; Marras, S.; Kamino, B. A.; Miranda, L.; De Angelis, F.; et al. Solution Synthesis Approach to Colloidal Cesium Lead Halide Perovskite Nanoplatelets with Monolayer-Level Thickness Control. *J. Am. Chem. Soc.* **2016**, *138* (3), 1010–1016.
- (36) Wu, Y.; Wei, C.; Li, X.; Li, Y.; Qiu, S.; Shen, W.; Cai, B.; Sun, Z.; Yang, D.; Deng, Z.; Zeng, H. In Situ Passivation of PbBr₆-Octahedra toward Blue Luminescent CsPbBr₃ Nanoplatelets with Near 100% Absolute Quantum Yield. *ACS Energy Lett.* **2018**, *3* (9), 2030–2037.
- (37) Acharyya, P.; Pal, P.; Samanta, P. K.; Sarkar, A.; Pati, S. K.; Biswas, K. Single Pot Synthesis of Indirect Band Gap 2D CsPb₂Br₅ Nanosheets from Direct Band Gap 3D CsPbBr₃ Nanocrystals and the Origin of Their Luminescence Properties. *Nanoscale* **2019**, *11* (9), 4001–4007.
- (38) Yang, D.; Zou, Y.; Li, P.; Liu, Q.; Wu, L.; Hu, H.; Xu, Y.; Sun, B.; Zhang, Q.; Lee, S. T. Large-Scale Synthesis of Ultrathin Cesium Lead Bromide Perovskite Nanoplates with Precisely Tunable Dimensions and Their Application in Blue Light-Emitting Diodes. *Nano Energy* **2018**, *47*, 235–242.